PERGAMON

International Journal of Heat and Mass Transfer 43 (2000) 1859–1868

International Journal of HEAT and MASS TRANSFER

www.elsevier.com/locate/ijhmt

Study on laminar film-wise condensation for vapor flow in an inclined small/mini-diameter tube

Bu-Xuan Wang*, Xiao-Ze Du

Thermal Engineering Department, Tsinghua University, Beijing 100084, China

Received 15 May 1999

Abstract

The correlating factors for flow condensation in small/mini-diameter tubes are analyzed by energy consideration. Based on the in-situ interface configuration, an analytical model is proposed for predicting the heat transfer characteristics. Both analytical and experimental results show that gravity has a decreasing effect on flow condensation in small/mini tubes. The inclination angle affects condensation heat transfer mainly by distributing gravity in stratifying the fluids and thinning the liquid film. In larger tubes, the former may become the main reason for heat transfer enhancement, especially in high vapor quality zone and at low inlet vapor Reynolds number. Comparison with the experimental data indicates that the proposed analytical model has a good capability for predicting flow condensation heat transfer in small/mini-diameter tubes.

Keywords: Laminar flow; Filmwise condensation; Small/mini-diameter tubes; Experimental examination

1. Introduction

Much work has been done concerning laminar film condensation in/outside vertical/horizontal tubes since the earliest and fundamental work of Nusselt [1]. The assumptions of the Nusselt or revised Nusselt theory have been examined in more complete studies [2–5]. Some semi-empirical or empirical correlations for flow condensation were proposed and well applied in most traditional industrial fields, such as those of Shah [6], Traviss et al. [7] and Aker et al. [8]. However, the development of technology needs a more compact and efficient heat exchanger in many applications, where condensation takes place inside or outside along small- or mini-channels, such as the automotive air conditioners or life-support systems in space, and also, the recent advances for the micro mechanical systems (MMS). Recently, few researchers began to explore the flow condensation heat transfer and pressure drop in small hydraulic-diameter tubes [9–11]. Some peculiar characteristics for small-diameter tubes were found as a noted higher condensation heat transfer coefficient than that in a traditional larger tube. But the mechanisms of influence factors acting on the two-phase flow system in small/mini-diameter tubes are still far from being understood. As a result of decreasing the tube diameter, the bending effect of the condensing film could not be neglected, which invalidated the "plate" assumption in classical Nusselt analysis. Rohsenow [12] already suggested that, only for tubes of diameter larger than 3 mm, the condensate film can be taken as on a plate surface, i.e. the bending effect of condensate

* Corresponding author. Tel.: +86-19-6278-4530; fax: +86-10-6277-0209.

E-mail address: bxwang@mail.tsinghua.edu.cn (B.-X. Wang).

0017-9310/00/$ - see front matter
PII: S0017-9310(99)00256-2

Nomenclature

A	cross-sectional area
d_i	inner diameter of test tube
E	energy
g	gravity acceleration
h	heat transfer coefficient
h_{lv}	latent heat
m'	mass flux
Nu	Nusselt number
p	pressure
r	radial coordinate
R	radius of test tube
Re	Reynolds number
S	the contract area between phases
T	temperature
u	velocity
x	vapor quality
z	axial coordinate

Greek symbols

β	inclination angle
δ	thickness
λ	thermal conductivity
μ	dynamic viscosity
ρ	density
σ	surface tension
φ^*	phase-change interface curvature angle

Subscripts

0	initial
k	kinetic
l	liquid
lv	vapor–liquid interface
min	thin film adhere to the top wall tube
p	potential
s	surface for energy, or saturate state for temperature
t	total
v	vapor
w	tube wall

Superscripts

-	average values

film can be neglected. For flow condensation in a smaller diameter tube, this may indicate that the shear stress and surface tension on a vapor–liquid interface would have a more obvious effect on the condensation process than that of the gravitational force. Such characteristics of a small/mini-diameter tube invalidate some hypotheses of classical or revised Nusselt theory. So, the correlations for flow condensation of a conventional-scale tube would not be applied to a mini-scale tube.

It is the purpose of the present paper to explore the flow condensation heat transfer characteristics in tubes with different inclinations and diameters of less than 5 mm, and to discuss the effects of the various forces on the condensation process. By providing an exact method of analyzing flow condensation in a mini-diameter tube, the analytical and experimental results reported here will be helpful for understanding the flow condensation heat transfer in small/mini-scale conditions.

2. Theoretical analysis

2.1. Phase-change interface configuration

The physical model of the problem is illustrated in Fig. 1. We assume that most of the condensate accumulates at the bottom of the tube by gravity and the phase-change interface may approach a lunar configuration by the additional cooperative effect of shear stress and surface tension, to take an arch with center at point O'. Also, the condensate may form a thin liquid film adhering to the top part of the tube by a capillary force as shown. In spite of various factors influencing the flow regimes, all of them can be embodied by the forces that act on the two-phase flow system. Therefore, by exploring the effect of the forces in different flow and geometrical conditions, we can reliably determine the in-situ flow regime. Brauner et al. [13] employed energy considerations to predict the interface configuration of a two-phase flow system with small density difference, but the shear stress effect was neglected, and hence, the reliability of predicted results for vapor–liquid flow systems would be questionable. The analysis is revised here, for predicting the vapor–liquid interfacial configuration.

In the case of flow condensation, the two-phase flow system in a horizontal or inclined tube is cooperated by gravity, shear stress and surface tension on the phase interface, i.e. the tube-wall surface and the vapor–liquid interface. The gravity perpendicular to the flow direction causes the stratifying of phases, while the other two lead to the condensate distributing uniformly along the circumference [14,15]. The resulted potential energy, E_p, from the component of the grav-

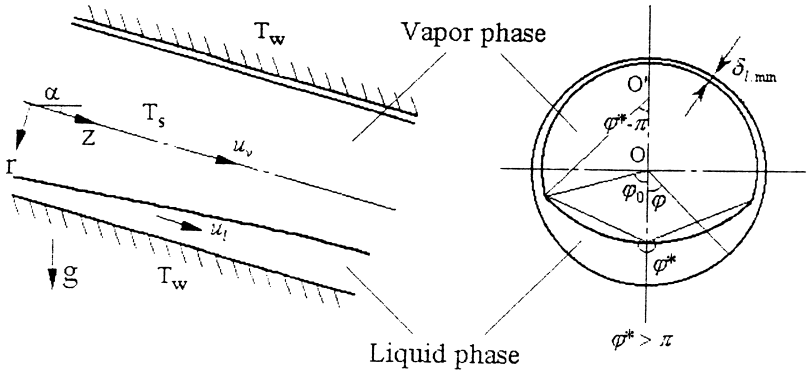

Fig. 1. Physical situation for flow condensation.

ity perpendicular to the flow direction, the kinetic energy, E_k, from the shear stress and the component of the gravity in the flow direction, and the surface energy, E_s, from the surface tension, constitute the energy system. For unit length of an inclined tube, the general relationship for the total energy, E_t, is given by:

$$E_t = E_p + E_s + E_k \tag{1}$$

among which,

$$E_p = \rho_l g \cos\beta A_i y_{gl} \tag{2}$$

$$E_k = \int_{-\varphi_0}^{\varphi_0}\int_{R-\delta_l}^{R} \frac{1}{2}\rho_l u_l^2 r \, dr \, d\varphi = \frac{1}{2}\rho_l A_l \bar{u}_l^2 \tag{3}$$

and

$$E_s = \sigma_{lv} S_{lv} \tag{4}$$

If the cross-section area of condensate, A_l, is determined, all the geometric parameters, including the distance from the condensate gravity center to the tube center O, y_{gl}, the contact area between liquid and vapor phases, S_{lv}, and the condensate film thickness at different φ for $-\varphi_0 < \varphi < \varphi_0$, δ_l, can be expressed as a function of the vapor–liquid interface curvature angle, φ^* [13].

According to the minimum energy principle, the steady in-situ interfacial configuration corresponds to the minimum of the total system energy, i.e.

$$\frac{dE_t}{d\varphi^*} = 0 \tag{5}$$

At the initial stage of flow condensation, our visual observation found that the flow pattern is concentric annular flow. So the thickness of liquid film adhere to the top area of the tube, $\delta_{l,min}$, can be determined as to satisfy the condition that the energy of annular flow is less than that of stratified flow with lunar interface configuration. We assume this thickness kept constant during the condensation process.

2.2. Analytical model for flow condensation

Besides those mentioned above for analyzing interfacial configuration, the basic assumptions are made below:

1. There are no interfacial waves between the condensate and vapor.
2. There is no presence of non-condensable gas.
3. The liquid film is assumed in its steady laminar flow, the convective terms in an energy equation and the inertia terms of a momentum equation being neglected.
4. The density and thermal conductivity of condensate in film are constants, respectively.

As a function of the inclination angle, α, the gravitational force could be divided into two components, that contribute to drive the film flow direction $g_z = g \sin\beta$ and to stratify the vapor and condensate $g_r = g \cos\beta$, respectively. Then, the governing equations for momentum and heat transfer can be expressed as:

$$\mu_l \frac{\partial^2 u_l}{\partial r^2} + \frac{1}{r}\mu_l \frac{\partial u_l}{\partial r} - \frac{dp_l}{dz} + \rho_l g_z = 0 \tag{6}$$

with boundary conditions

$$u_l = 0, \quad \text{for } r = R \tag{7a}$$

$$-\mu_l \frac{\partial u_l}{\partial r} = \tau_{lv}, \quad \text{for } r = (R - \delta_l) \tag{7b}$$

among which, for a determined vapor–liquid interface curvature angle by energy consideration, φ^*, if $-\varphi_0 < \varphi < \varphi_0$, δ_l will be the function of z and φ, i.e. $\delta_l = \delta(z, \varphi)$; else, $\delta_l = \delta_{l,min}$:

$$h_{\mathrm{lv}}\frac{\mathrm{d}m_{\mathrm{l}}'}{\mathrm{d}z}=\int_0^{2\pi}\frac{(T_{\mathrm{s}}-T_{\mathrm{w}})\mathrm{d}\varphi}{\ln\dfrac{R+\delta_{\mathrm{w}}}{R}\dfrac{1}{\lambda_{\mathrm{w}}}+\ln\dfrac{R}{R-\delta_{\mathrm{l}}}\dfrac{1}{\lambda}} \tag{8}$$

$$m_{\mathrm{l}}'+m_{\mathrm{v}}'=m_{\mathrm{v0}}' \tag{9}$$

From Eq. (6), together with the boundary conditions, yields

$$u_{\mathrm{l}}(z,r,\varphi)=\frac{2}{2\mu_{\mathrm{l}}}\left(\frac{\mathrm{d}p_{\mathrm{l}}}{\mathrm{d}z}-\rho_{\mathrm{l}}g_z\right)\left[\frac{r^2-R^2}{2}-(R-\delta)^2\ln\frac{r}{R}\right]-\frac{\tau_{\mathrm{lv}}(R-\delta_{\mathrm{l}})}{\mu_{\mathrm{l}}}\ln\frac{r}{R} \tag{10}$$

Thus, the mass flux of liquid would be

$$m_{\mathrm{l}}'(z)=\int_{-\varphi_0}^{\varphi_0}\mathrm{d}\varphi\int_{R-\delta(z,\,\varphi)}^{R}\rho_{\mathrm{l}}u_{\mathrm{l}}(z,r,\varphi)\mathrm{d}r \tag{11}$$

We can obtain another expression of mass flux from Eq. (8) as

$$m_{\mathrm{l}}'(z)=\frac{1}{h_{\mathrm{lv}}}\int_0^z\frac{(T_{\mathrm{s}}-T_{\mathrm{w}})(2\pi-2\varphi_0)}{\ln\dfrac{R+\delta_{\mathrm{w}}}{R}\dfrac{1}{\lambda_{\mathrm{w}}}+\ln\dfrac{R}{R-\delta_{\mathrm{l,\,min}}}\dfrac{1}{\lambda_{\mathrm{l}}}}\mathrm{d}z+\frac{1}{h_{\mathrm{lv}}}\int_0^z\int_{-\varphi_0}^{\varphi_0}\frac{T_{\mathrm{s}}-T_{\mathrm{w}}}{\ln\dfrac{R+\delta_{\mathrm{w}}}{R}\dfrac{1}{\lambda_{\mathrm{w}}}+\ln\dfrac{R}{R-\delta(z,\varphi)}\dfrac{1}{\lambda_{\mathrm{l}}}}\mathrm{d}\varphi\,\mathrm{d}z \tag{12}$$

The average liquid velocity, $\bar{u}_{\mathrm{l}}$, will be:

$$\bar{u}_{\mathrm{l}}=m_{\mathrm{l}}'(z)/\rho_{\mathrm{l}}/A_{\mathrm{l}} \tag{13}$$

and the average velocity of vapor flow can be yielded from Eq. (9) as

$$\bar{u}_{\mathrm{v}}(z)=[\pi R^2\rho_{\mathrm{v}}u_{\mathrm{v0}}-m_{\mathrm{l}}'(z)]/[(\pi R^2-A_{\mathrm{l}})\rho_{\mathrm{v}}] \tag{14}$$

The vapor quality can be obtained by

$$x=\frac{m_{\mathrm{v0}}'-m_{\mathrm{l}}'(z)}{m_{\mathrm{v0}}'} \tag{15}$$

Neglecting the inertia effect, the pressure drop of liquid film will be:

$$\frac{\mathrm{d}p_{\mathrm{l}}}{\mathrm{d}z}=\rho_{\mathrm{v}}g\,\sin\beta-\frac{\displaystyle\int_{-\varphi_0}^{\varphi_0}\tau_{\mathrm{lv}}(z,\varphi)[R-\delta(z,\varphi)]\mathrm{d}\varphi}{\pi R^2-A_{\mathrm{l}}}-\frac{\tau_{\mathrm{lv}}(z)(2\pi-2\varphi_0)R}{\pi R^2-A_{\mathrm{l}}} \tag{16}$$

Shear stress on the vapor–liquid interface was given by Faghri and Chow [16] as

$$\tau_{\mathrm{lv}}(z,\varphi)=\frac{c_{\mathrm{f}}}{2}\rho_{\mathrm{v}}[\bar{u}_{\mathrm{v}}(z)-u_{\mathrm{l}}(z,R-\delta_{\mathrm{l}},\varphi)]^2+\frac{1}{R-\delta_{\mathrm{l}}}\frac{\partial^2 m_{\mathrm{l}}'(z)}{\partial z\,\partial\varphi}[\bar{u}_{\mathrm{v}}(z)-u_{\mathrm{l}}(z,R-\delta_{\mathrm{l}},\varphi)] \tag{17}$$

The average vapor velocity is far greater than the liquid velocity at the vapor–liquid interface, and so, $u_{\mathrm{l}}(z,\,R-\delta_{\mathrm{l}},\,\varphi)$ in Eq. (17) can be neglected.

2.3. Numerical scheme

The proposed physico-mathematical model can be solved numerically. For a given tube size and inlet vapor Reynolds number, Re_{v0}, the discretizations of governing equations were taken along the axis and periphery, respectively. The step size in the z-direction is unknown at the beginning, while the step size taken in the circumference direction was $\Delta\varphi=0.1^\circ$.

At first, the condensate film thickness, $\delta(z_{\mathrm{i}},\,\varphi_{\mathrm{i}})$, is determined by assumed liquid cross-section area, $A_{\mathrm{l,i}}$, and the first-guess values of the interface curvature angle, φ_{i}^*, at every axial step. Calculating the shear stress on the vapor–liquid interface by Eq. (17) using the last average vapor velocity. Then, the equation for the momentum conservation of liquid, Eqs. (6) and (7), is solved when combined with Eq. (16).

If the energy system acquired by Eqs. (1)–(4) is not satisfied with the minimum energy principle, slightly change the estimated interface curvature angle, φ_{i}^*, and repeat the steps.

Balancing Eqs. (11) and (12), the step size of the axial position, Δz_{i}, can be acquired, and therefore, the vapor quality, x, and average vapor velocity, $\bar{u}_{\mathrm{v}}(z_{\mathrm{i}})$, can be calculated by Eqs. (14)–(15). The whole iterative process is repeated until the value of $\bar{u}_{\mathrm{v}}(z_{\mathrm{i}})$ are satisfied with the required precision. Then, the corresponding condensation heat transfer characteristics are solved as

$$h(z_{\mathrm{i}},\varphi_{\mathrm{i}})=\frac{1}{\left[\ln\dfrac{R+\delta_{\mathrm{w}}}{R}\dfrac{1}{\lambda_{\mathrm{w}}}+\ln\dfrac{R}{R-\delta_{\mathrm{l}}(z_{\mathrm{i}},\varphi_{\mathrm{i}})}\dfrac{1}{\lambda_{\mathrm{l}}}\right]R} \tag{18}$$

Thereby, the average local Nusselt number Nu can be calculated as

$$Nu(z_{\mathrm{i}})=\frac{1}{2\pi}\int_0^{2\pi}\frac{2h(z_{\mathrm{i}},\varphi_{\mathrm{i}})R}{\lambda_{\mathrm{l}}}\mathrm{d}\varphi \tag{19}$$

3. Experimental setup

A two-phase flow loop is built for conducting the

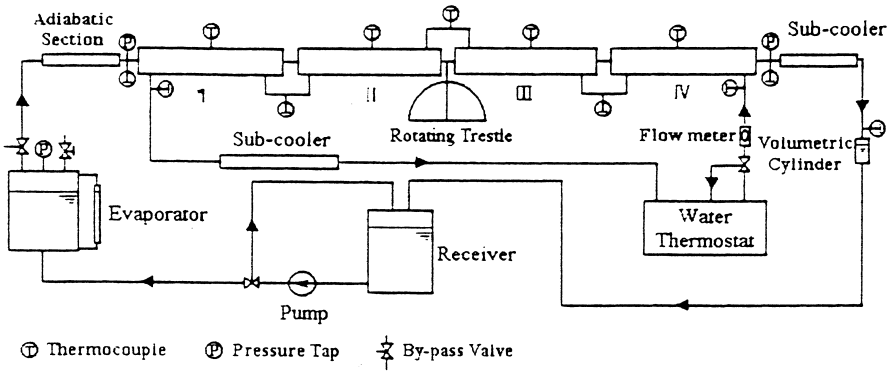

Fig. 2. Schematic diagram of the test setup.

condensation experiments. The experimental setup is shown in Fig. 2. Water vapor (steam) was used as the test fluid. In order to explore the effects of various forces more obviously, a relatively low range of mass flux rates (10–100 kg/s m^2) was used for tests.

The test setup, shown in Fig. 2, consists of two main loops, namely, the vapor-condensate loop and the cooling water loop. The cleaned water stored in the receiver is pumped into the evaporator. The by-pass line at the discharge side of the pump enables the regulation of the liquid volume in the evaporator. The evaporator is an electric boiler of which the power can vary from 0–3 kW. The flow rate of superheated or saturated vapor generated by the evaporator is adjusted by another by-pass valve at the outlet. The vapor passes through the adiabatic section to come out in a saturated/superheated condition. It is then condensed in the test section to a saturated condition. Transparent tubes are connected to both ends of the test section to visually inspect the flow pattern. The outlet condensate flows through the sub-cooling section to reach a subcooled condition, and comes into the volumetric cylinder to get the volumetric flow rate. It is finally collected to the liquid receiver.

The cooling water loop for condensing the vapor contains a water thermostat bath with adjustable temperature ranging from 40 to 100°C. A by-pass valve is provided to adjust the flow rate which is measured by a flowmeter or by weighing the cooling water collected at a certain time for different ranges.

The test section consists of four tube-in-tube condensers with counterflow arrangement, denoted as I, II, III, IV, respectively, in Fig. 2, each of which is 300 mm long. The test section is mounted on a pivoted beam truss supported at the center with rigid adjustable fixtures, and so it can be altered for different inclinations. The inclination angle, β, is taken as 0° when the test section is horizontal and $\beta=90°$ for the vapor flow parallel to the gravity. The vapor flows through the inner test tube while the cooling water flows into the annulus through a mixer in the opposite direction, as shown in Fig. 3(a). Four different sized copper pipes were selected as the inner tubes with inside diameters of 1.94, 2.80, 3.95, 4.98 mm and corresponding

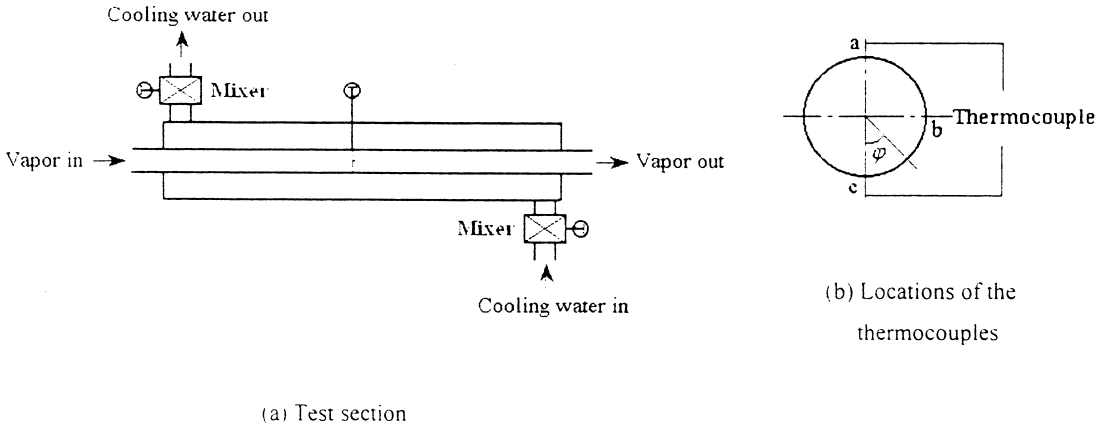

(a) Test section

(b) Locations of the thermocouples

Fig. 3. Details of test section. (a) Test section. (b) Locations of the thermocouples.

Table 1
Range of operating conditions

Parameter	Range
Vapor mass flow rate [kg m^{-2} s^{-1}]	11.3–94.5
Vapor inlet Reynolds number, Re_{v0}	4.5×10^3–1.4×10^4
Vapor inlet pressure [kPa]	1077–1521
Vapor inlet superheat [°C]	0.34–5.41
Condensate outlet subcooling [°C]	0.0–9.44
Temperature drop between the vapor and wall [°C]	1.23–6.71
Vapor inlet quality	1.0
Vapor outlet quality	0.0–0.2

outside diameters of 2.95, 4.95, 5.98, 6.98 mm, respectively. The outer tube is 11.97 mm i.d. and is covered by a layer of insulation on the outer wall.

The temperature and pressure of the vapor/condensate were measured at both ends of the whole test section. The inlet and outlet temperatures of cooling

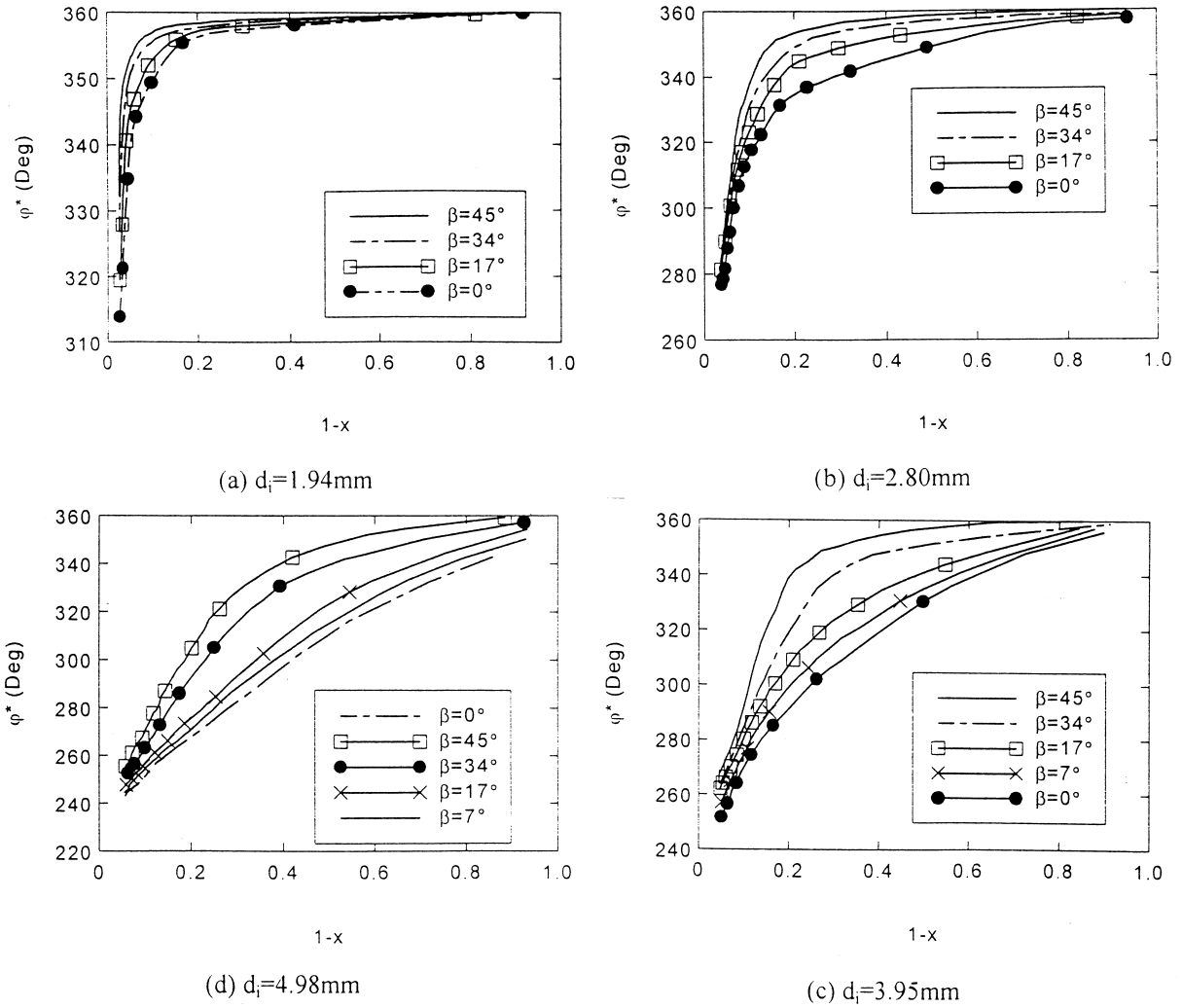

Fig. 4. Predicted variation of the vapor–liquid interface curvature angle with liquid quality for different inclination angles and test tubes: (a) $d_i = 1.94$ mm; (b) $d_i = 2.80$ mm; (c) $d_i = 3.95$ mm; (d) $d_i = 4.98$ mm.

water for each of the separate condensers and the condensate temperature in the volumetric cylinder were also measured. As shown in Fig. 3(b), at each middle location of the four separate condensers, the outer wall temperatures of the test tube were measured at three points, a, b, c, corresponding to $\varphi = 0$, 90 and 180°, respectively. Their arithmetic mean was taken as the average surface temperature. All the temperatures were measured by the calibrated 0.1 mm T-type copper–constantan thermocouples with an accuracy of 0.1°C. The pressures were measured by a pressure gauge with an accuracy of ±0.25%. The weighing accuracy of cooling water is 0.1 g, while the accuracy of the volumetric cylinder is 0.1 ml.

The outer wall of the test tube was treated with mechanical polishing and the inner wall of the tube was washed by acetone repeatedly to avoid organic and dirt contamination. At most test conditions, the error of heat balance between sensible heat of cooling water and latent heat of condensate is less than 5%. For the uncertainty analysis, the basic methodology of Kline and McClintock [17] was adopted. The average uncertainty in the measurement of the present experiments was estimated as ±25%.

4. Results with discussion

Five data sets were measured corresponding to the different inclination angles, $\beta = 0$, 7, 17, 34 and 45°, respectively. The details of operating conditions are summarized in Table 1.

Fig. 4 shows the analytical predictions of the present model to compare the variation of vapor–liquid interface curvature angle, φ^*, with different liquid quality, $(1-x)$, and tube inclination angle, β, for different test tubes. Such a variation of φ^* indicates the effects of various forces on flow condensation as mentioned above in the theoretical analysis. The cross-sectional area of liquid film increases with increasing liquid quality, and therefore, surface energy takes a more important role in energy balance, as to increase φ^*. Decreasing test tube diameter, d_i, may enhance the influence of surface tension on shaping the interface configuration according to the Young–Laplace equation, but also will enlarge the vapor velocity and cause a more obvious influence of shear stress on the flow. This means the surface energy and kinetic energy play a more important role in a system's total energy consideration, and hence, as shown in Fig. 4, the variation of the inclination angle has much less effect on the interface curvature in a 1.94 mm i.d. tube than that in larger tubes. Since the inclination angle changes the gravity component on stratifying fluids, this may indicate that gravity does not play an important role in shaping the flow regime in a small/mini diameter tube.

Increasing vapor velocity can weaken the fluids stratifying, i.e., increase the interface curvature angle φ^*, as shown in Fig. 5. It is further evident that the shear stress of the vapor has the contrary effect on shaping the vapor–liquid interface configuration with a gravity component perpendicular to the flow direction.

The experimental results, plotted in Fig. 6, show the variation of the average local Nusselt number, Nu, with liquid quality, $(1-x)$, at different inclination angles for the same inlet vapor Reynolds number, $Re_{v0} = 4500$. The variation of the tube inclination angle, β, brings no obvious change to Nu for the 1.94 mm i.d. tube, indicating little effect of gravity on flow condensation. The effect of the inclination angle increases with increasing tube diameter. However, the inclination angle has quite complicated effects on Nu for different sized tubes. For tubes of 1.94 and 2.80 mm i.d., the Nusselt number increases basically with increasing tube inclination, although not very obviously. For two other larger tubes of 3.95 and 4.98 mm i.d., the inclination angle has different effects on Nu for different quality zones: Nu decreases with increasing inclination if the liquid quality is lower than 0.4–0.6, and Nu increases with increasing inclination if liquid quality is larger than 0.4–0.6. But in general, Nu is always the largest for flow condensation in the horizontal tubes ($\beta = 0°$).

As mentioned above, in an inclined tube, gravity is divided into two components, stratifying the fluids and driving the condensate film flow, respectively. For a small/mini-diameter tube, the gravity has little effect on stratifying the vapor–liquid two-phase flow, the main influence of gravity on condensation will be to

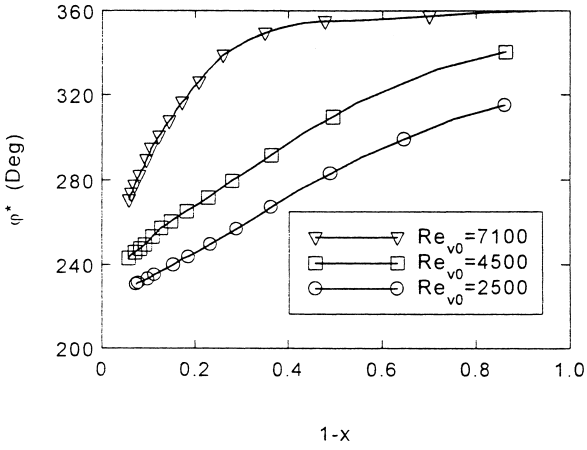

Fig. 5. Variation of the vapor–liquid interface curvature angle with vapor quality for a different inlet Reynolds number ($d_i = 4.98$ mm, $\beta = 0°$).

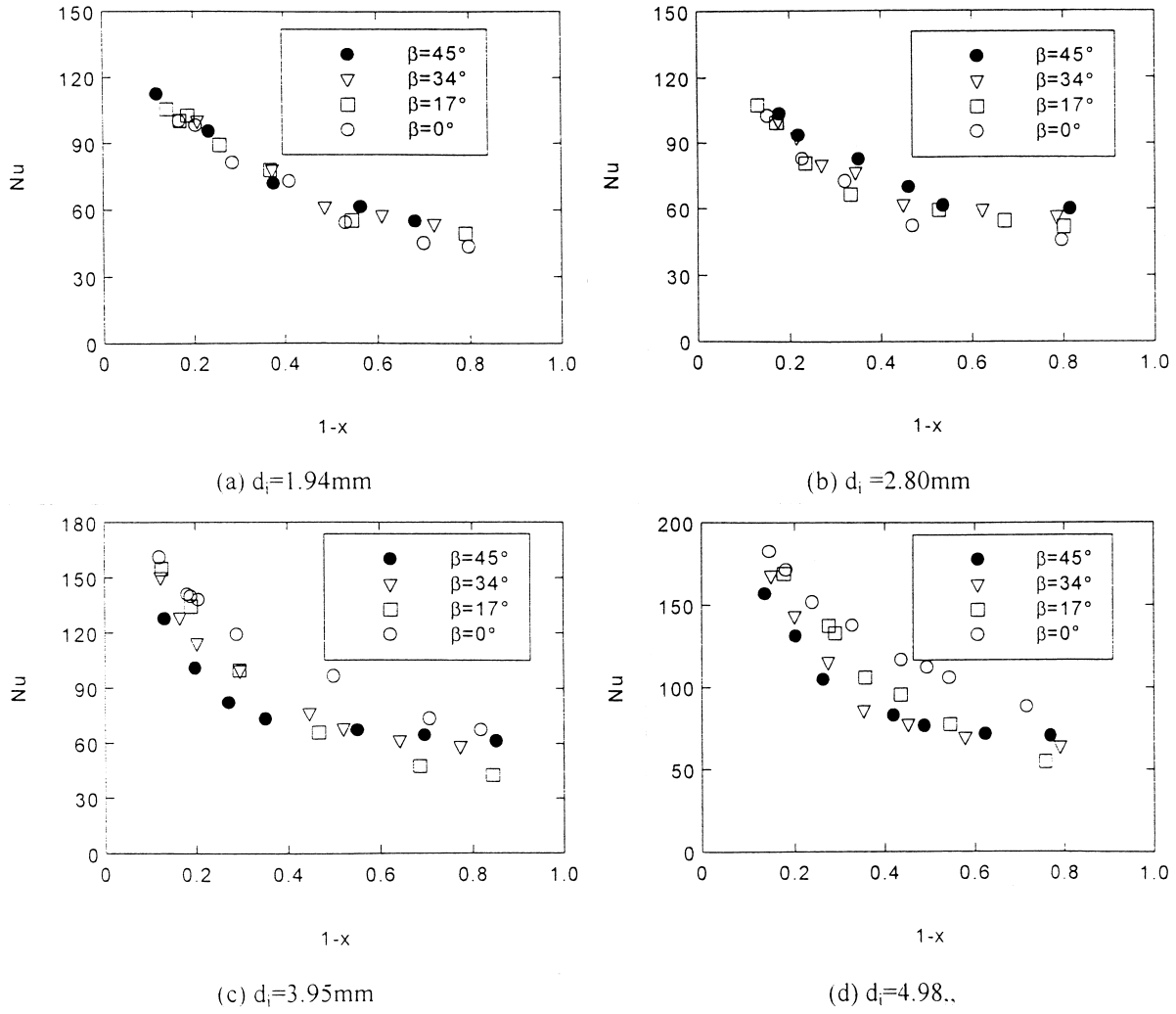

Fig. 6. Measured variation of local Nu with liquid quality for different inclination angles and test tubes ($Re_{v0}=4500$): (a) $d_i=1.94$ mm; (b) $d_i=2.80$ mm; (c) $d_i=3.95$ mm; (d) $d_i=4.98$ mm.

enhance heat transfer by thinning the condensate film, which becomes obvious with increasing the tube inclination. For larger tubes, at the beginning of the condensation process, the fluids are stratified obviously, corresponding to smaller φ^* in Fig. 4(c) and (d), which enlarges the contact area between the vapor and thin condensate film. As the vapor quality, x, descends along the flow path, the condensate film becomes thicker accordingly, and hence, the gravity component along the flow direction has more effect on heat transfer enhancement, i.e. Nu increases with an increasing inclination angle. For a horizontal tube, the stratification of vapor and liquid may lead to a clear enhancement of condensation heat transfer.

The heat transfer enhancement of stratifying the fluids and thinning the condensate film by gravity can be illustrated by Fig. 7. Gravity has little effect on flow condensation in the smaller diameter tubes, the experimental results show that Nu increase with an increasing inlet vapor Reynolds number. Both decreasing the tube diameter and increasing the inlet Reynolds number will weaken the fluids stratifying effect by gravity, while in contrast, the film thinning effect by the vapor shear stress will become the dominant reason of heat transfer enhancement. For larger tubes of 3.95 and 4.98 mm i.d., with an inlet Reynolds number, $Re_{v0} \approx 4.5 \times 10^3$, Nu is obviously larger than that with higher inlet Reynolds numbers conditions. The interface curvature angle, shown in Fig. 5, is quite small in such small Re_{v0}, that the enlargement of the contact area between the vapor and thin condensate film can obviously enhance heat transfer.

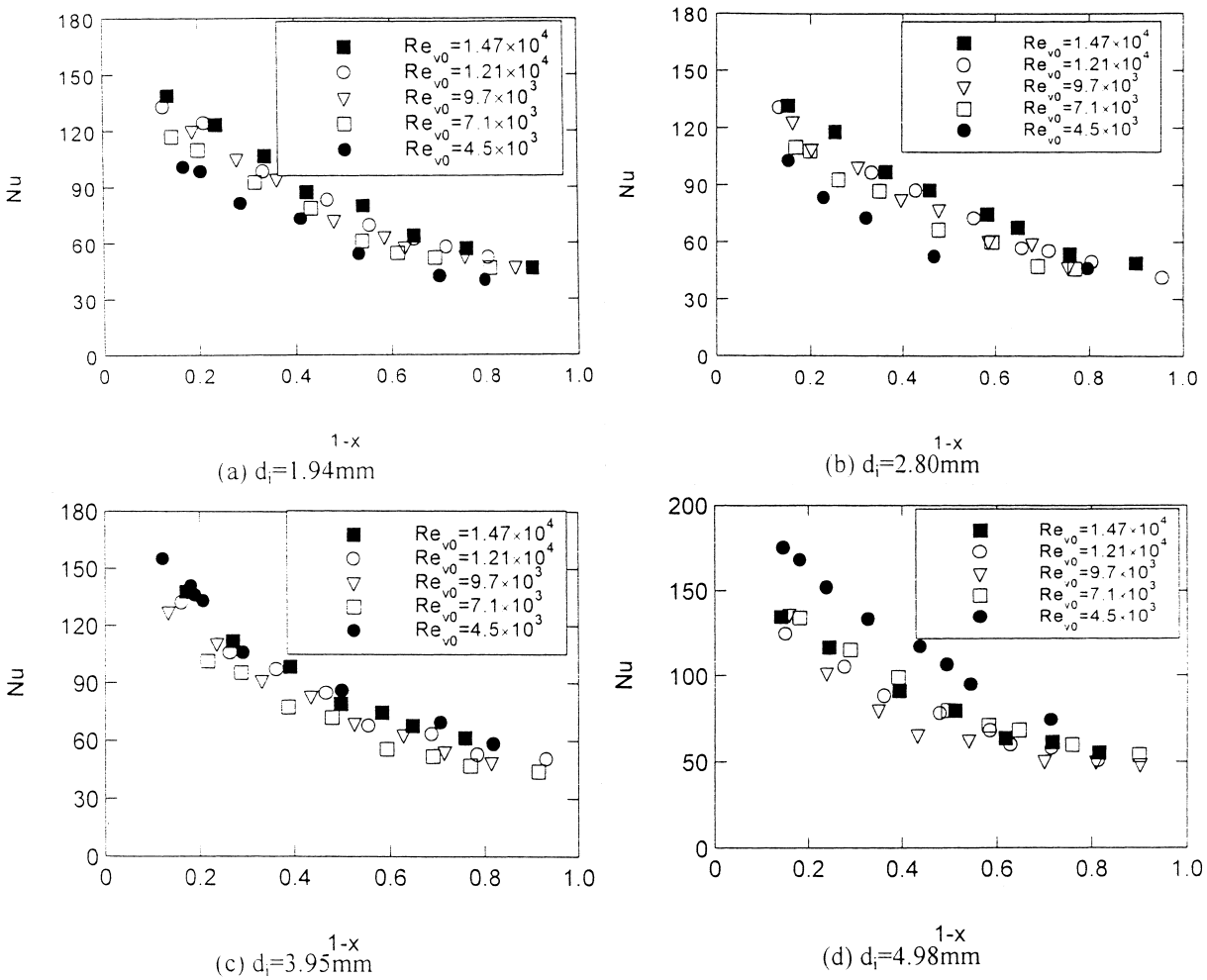

Fig. 7. Measured variation of local *Nu* with liquid quality for a different inlet vapor Reynolds number in horizontal tubes ($\beta=0°$): (a) $d_i=1.94$ mm; (b) $d_i=2.80$ mm; (c) $d_i=3.95$ mm; (d) $d_i=4.98$ mm.

Fig. 8 shows the comparison of the analytical model developed for prediction with the experimental results. The deviations are within a range of −28 to +20%. As the uncertainty of the present experimental measurement is estimated as about ±25%, the deviation of predicted and experimental results may indicate a little over-prediction of the analytical model. This may come from the assumption of a constant tube wall temperature, which does not satisfy the actual experimental conditions. Besides, the calculation of the thickness of the liquid film which adhere to the top area of the tube $\delta_{l,min}$, still needs to be improved.

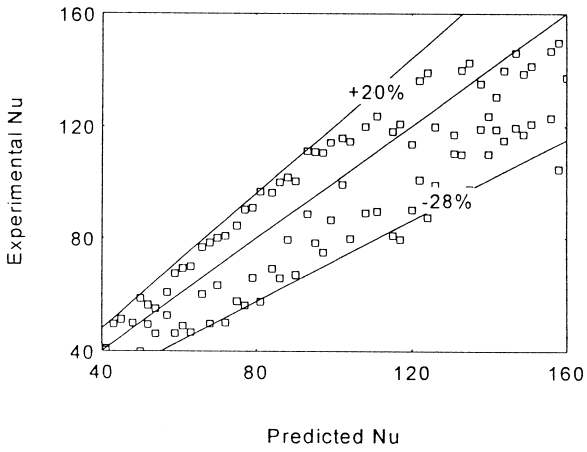

Fig. 8. Comparison of analytical model with experimental data.

5. Concluding remarks

The principle of energy consideration is employed to determine the phase-change interface configuration for

flow condensation in inclined small/mini-diameter tubes. Based on the boundary conditions obtained, an analytical model is developed for predicting the heat transfer characteristics. Experiments have been carried out to measure the heat transfer coefficients for different diameter tubes with various inclinations for relatively low inlet vapor Reynolds numbers Re_{v0}. Both the analytical prediction and the experimental results show that the effect of gravity on flow condensation decreases in small-diameter tubes, and the effect of the inclination angle on condensation heat transfer will be mainly to distribute gravity in stratifying the fluids and thinning the liquid film. As gravity takes a more obvious effect on flow condensation in larger tubes, the former may become the main heat transfer enhancement reason, especially in a high vapor quality zone and at a low inlet vapor Reynolds number. Comparison with the experimental data indicates that the proposed analytical model is capable of good prediction, although it seems a slight over-prediction.

Acknowledgements

The current financial support for this research project from the National Natural Science Foundation of China (Grant No. 59995550-3) is gratefully acknowledged.

References

[1] W. Nusselt, Die Oberflächenkondensation des Wasserdampfes, Ver. Deut. Ing. 60 (1916) 541–546.
[2] J.W. Rose, Condensation heat transfer fundamentals, Trans. IChemE 76 (1998) 143–152.
[3] J.W. Rose, Effect of pressure gradient in force convection film condensation on a horizontal tube, Int. J. Heat Mass Transfer 27 (1984) 39–47.
[4] K. Suzuki, Y. Hagiwara, H. Izumi, A numerical study of forced-convective filmwise condensation in a vertical tube, JSME Int. J., Ser. II 33 (1990) 134–140.
[5] W.M. Rohsenow, J.H. Weber, A.T. Ling, Effect of vapor velocity on laminar and turbulent-film condensation, Trans. ASME 78 (1956) 1637–1643.
[6] M.M. Shah, A general correlation for heat transfer during film condensation inside pipes, Int. J. Heat Mass Transfer 22 (1979) 547–556.
[7] D.P. Traviss, W.M. Rohsenow, A.B. Baron, Forced-convective condensation in tubes: a heat transfer correlation for condenser design, ASHRAE Trans. 79 (1973) 157–165.
[8] W.W. Aker, H.F. Rossen, Condensation inside a horizontal tube, Chem. Eng. Prog. Symp. Ser. 30 (1960) 145–149.
[9] C.Y. Yang, R.L. Webb, Condensation of R-12 in small hydraulic diameter extruded aluminium tubes with and without micro-fins, Int. J. Heat Mass Transfer 39 (1996) 791–800.
[10] C.Y. Yang, R.L. Webb, Friction pressure drop of R-12 in small hydraulic diameter extruded aluminium tubes with and without micro-fins, Int. J. Heat Mass Transfer 39 (1996) 801–809.
[11] Y.-Y. Yan, T.-F. Lin, Condensation heat transfer and pressure drop of refrigerant R-134a in a small pipe, Int. J. Heat Mass Transfer 42 (1999) 697–708.
[12] W.M. Rohsenow, Film condensation, Applied Mechanics Reviews 23 (1970) 487–496.
[13] N. Brauner, J. Rovinsky, D.M. Maron, Determination of the interface curvature in stratified two-phase system by energy consideration, Int. J. Multiphase Flow 12 (6) (1996) 1167–1185.
[14] A. Murata, E. Hihara, T. Saito, Prediction of heat transfer by direct contact condensation at a steam-subcooled water interface, Int. J. Heat Mass Transfer 35 (1992) 101–109.
[15] M. Soilam, N.Z. Azer, Flow patterns during condensation inside a horizontal tube, ASHRAE Trans. 77 (1971) 210–224.
[16] A. Faghri, L.C. Chow, Annular condensation heat transfer in a microgravity environment, Int. Comm. Heat Mass Trans. 18 (1991) 715–792.
[17] S.J. Kline, F.A. McClintock, Describing uncertainties in single-sample experiments, Mech. Engng 75 (1953) 3–12.